Korean J. Chem. Eng., 38(6), 1117-1128 (2021)
DOI: 10.1007/s11814-021-0796-2

pISSN: 0256-1115
eISSN: 1975-7220

REVIEW PAPER

Recent progress on Al distribution over zeolite frameworks: Linking theories and experiments

Seung Jae Kwak*, Hyo Seok Kim*, Namjun Park*, Myung-June Park,***,†, and Won Bo Lee*,†**

*School of Chemical and Biological Engineering, Seoul National University, Seoul 08826, Korea
**Department of Chemical Engineering, Ajou University, Suwon 16499, Korea
***Department of Energy Systems Research, Ajou University, Suwon 16499, Korea
(*Received 26 November 2020 • Revised 26 March 2021 • Accepted 4 April 2021*)

Abstract−The location and distribution of aluminum in zeolites is considered important in determining various properties, such as acidity and reactivity. Controlling the placement of aluminum substitution has therefore been of significant interest, and a number of studies have been conducted, including synthesis methods using either different organic structure-directing agents (OSDAs) or cationic species, and the application of dealumination as post-processing. In addition to experimental developments, computational methods have emerged as a useful tool for analyzing the effects of different types of aluminum siting on catalytic properties, especially by incorporating statistical methods. A review of recent developments and findings related to aluminum siting and its effects is presented in this work. Analysis of the thermodynamic distribution of aluminum, as well as synthetically altered distribution in different zeolite frameworks, has been discussed. Computational studies have revealed that catalytic properties are sensitive to adsorbate-dependent properties such as the size of rings and voids for the residence of aluminum, the relative distribution of acid sites, and the adsorption properties of molecules in different framework motifs. Along with the atomic scale evaluation of synthetic treatments in positioning the aluminum, cases of instrumental analysis methods and their verification with simulations is discussed, demonstrating how theories have complemented and, sometimes modified, experimental perspectives. Lastly, recent progress in incorporating machine learning techiques, its application to zeolites, and directions for future work are introduced.

Keywords: Zeolites, Acid Sites, Statistical Averaging, Computational Chemistry, Machine Learning

INTRODUCTION

Zeolites are known for their outstanding selective reactivity in the mediation of various chemical reactions and have taken deep root in the field of catalysis, ranging from petrochemical reactions to ion exchange, and gas separation [1]. The uniformity of unique microporous structures also makes them useful as molecular sieves. More than 200 unique zeolite frameworks have been identified, while many more theoretical structures are thought to exist [2].

Recent concerns regarding global warming and fossil fuel depletion have sparked interest in zeolites as potential catalysts for converting alternative sources, such as shale gas and biomass, to value-added products via C1-3 chemistry [3]. This feature fueled computational studies on the atomistic scale to investigate the structure and reactivity of various zeolites [4,5]. One of the directions for the application of computational power in this field is to devise a strategy to increase the reactivity of zeolites by exchanging particular silicon atoms with 3+ ions, most commonly aluminum (Al) atoms. Since the ground state energy of the structure can be obtained directly using density functional theory (DFT), the thermodynamic properties concerning the location of Al are predictable.

The accumulation of microscopic studies recently suggested methodologies that consistently link the results at the atomic scale (theory) to those on the real visible scale (experiment). An example is a statistical approach, where macroscopic properties can be determined as an ensemble of microscopic properties; individual DFT calculations at the atomic level can be considered to produce each of these ensembles and to provide the probability of its existence. Such calculations would require excessive computational effort, but recent hardware developments have resolved these issues to some extent.

In this study, some of the reported efforts to control Al siting and assess the role of Al placement in the field of zeolite science are reviewed. A brief introduction to zeolites and the commonly used statistical averaging is made, followed by a discussion on the catalytic significance of Al distribution. Research works that have focused on the thermodynamic placement of Al will be presented followed by synthesis methods for controlling Al distributions, such as organic structure-directing agents (OSDAs), incorporation of different cations, and dealumination post-processing, along with a theoretical analysis. Recent computational studies that have disputed common knowledge in the field of zeolites will be presented. In the last section, machine learning methods applied to zeolites and other heterogeneous catalysis are summarized, with emphasis on adequate structural representation methods.

STATISTICAL METHODS

Alumina silicates have different tetrahedral sites (T sites), each

†To whom correspondence should be addressed.
E-mail: mjpark@ajou.ac.kr, wblee@snu.ac.kr

containing four oxygens in the vicinity working as possible Brønsted acid sites (BAS), and the catalytic properties are highly dependent on the locations of the BAS site, that is, the geometric conditions in which the reactants are situated. Although many researchers have attributed this feature to different strengths of acid sites in the past, recent studies have found that the degree of difference in acidic strength is small, indicating that the variance of the catalytic property may result from the probabilistic distribution of protons [6]. This motivated the application of statistical averaging to calculate all or a large portion of energies allocated to different Al and BAS locations, and the significant increase in computational power and the advent of efficient algorithms has now enabled the implementation of the approach. Boltzmann averaging of different properties can be computed on the basis of the energies, as follows [7]:

$$\langle E_{ZA}\rangle = \frac{\Sigma_i^n\left[E_{ZA,i}\exp\left(-\frac{G_{ZA,i}}{k_BT}\right)\right]}{\Sigma_i^n\left[\exp\left(-\frac{G_{ZA,i}}{k_BT}\right)\right]} \quad (1)$$

where $\langle E_{ZA}\rangle$ represents the averaged property of interest, and $E_{ZA,i}$ and $G_{ZA,i}$ denote the specific property and Gibbs free energy, respectively, in the *i*-th site. The symbols, k_B and T, represent the Boltzmann constant and temperature, respectively.

The statistical approach based on averaging offers a realistic link between theoretical calculations and the experimentally observed zeolite properties. For example, by averaging over the four BAS sites for each Al placement, properties such as site-specific acidity can be obtained, while averaging over all possible Al placements provides a framework-specific property of thermodynamically natural distribution of Al.

WHY IS Al SITING IMPORTANT ?

The conversion of dimethyl ether (DME) to methyl acetate (MA) in the 8-membered ring (8MR) is considered as an example to show the dependence of catalytic reactivity on the position and distribution of Al in the zeolite. Cheung et al. reported that H-mordenite (H-MOR) and H-ferrierite (H-FER) zeolite catalyzed the conversion of DME to MA with a stable reaction rate and >99% selectivity at low temperatures (423-463 K) [8]. The reaction mechanism was suggested as follows:

$$R_1: Z\text{-}H+DME \rightarrow Z\text{-}CH_3+H_2O \quad (2)$$

$$R_2: Z\text{-}CH_3+CO \rightarrow Z\text{-}CH_3CO \quad (3)$$

$$R_3: Z\text{-}CH_3CO+DME \rightarrow Z\text{-}CH_3+MA \quad (4)$$

The methyl group produced by the dissociation of DME (R_1) combines with CO to form an acetyl group (R_2), which reacts with DME to produce MA (R_3). The rate-determining step (RDS) of the mechanism was verified to be R_2 by kinetic experiments and nuclear magnetic resonance (NMR) spectroscopy [9]. Bhan et al. found that the carbonylation reaction only occurred in the zeolites, which consist of the 8MR site [10]. The number of BAS within 8MR channels was measured by the rigorous deconvolution of the infrared bands for BAS in H-MOR and H-FER, and the MA production rate was proportional to the number of BAS within 8MR.

Boronat et al. explained the attribute of the BAS in the 8MR cage of the zeolite using first-principles calculations on H-MOR [11]. The activation energies of the methyl group by four attacking molecules (CO, CH_3OH, DME, and H_2O) were calculated at each T-site in H-MOR, as follows:

$$R_4: Z\text{-}CH_3+CO \rightarrow Z^- + CH_3CO^+ \quad (5)$$

$$R_5: Z\text{-}CH_3+CH_3OH \rightarrow Z^- + (CH_3)_2OH^+ \quad (6)$$

$$R_6: Z\text{-}CH_3+DME \rightarrow Z^- + (CH_3)_3O^+ \quad (7)$$

$$R_7: Z\text{-}CH_3+H_2O \rightarrow Z^- + CH_3OH_2^+ \quad (8)$$

It was shown that DME could access the methyl group on the T sites to produce trimethyloxonium (R_6), except for the T3-O33 position, where the activation energy for R_6 is higher than that of R_4 due to the steric hindrance of DME resulting from the unusual orientation of the methyl group at T3-O33 in the 8MR, indicating that the unique selectivity appears only at the T3-O33 position.

The Al distribution can significantly influence the BAS in 8MR and the reactivity of the DME carbonylation reaction. Li et al. quantitatively verified that the formation rate of MA by DME carbonylation reaction is proportional to the concentration of BAS in 8MR [12], which could be controlled by introducing various organic structure-directing agents (OSDAs) for the synthesis of the H-MOR structure. It was also shown that the strength of the interaction between the amine or sodium cation and $[AlO_4]^-$ played an important role in the Al distribution. The stronger the interaction, the higher the number of Al in the 8MR, and the corresponding BAS concentration.

Jung et al. found that ferrierite zeolite synthesized by the seed-derived hydrothermal method without any OSDA had a high cat-

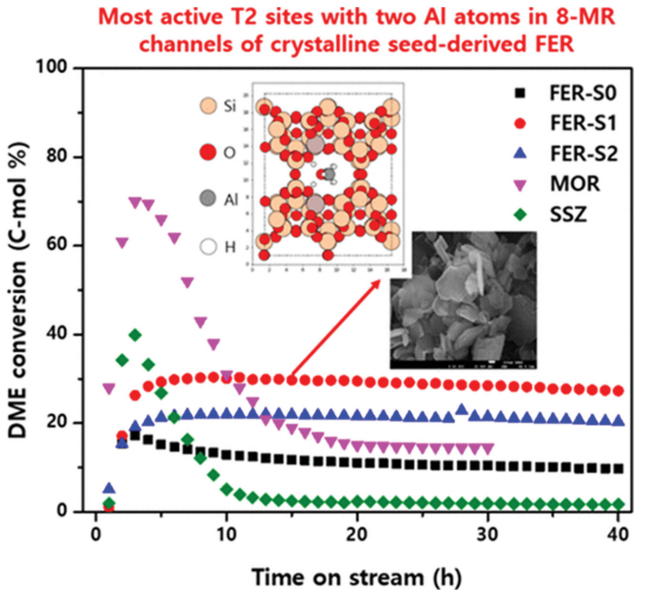

Fig. 1. DME conversion over seed-derived ferrierite zeolite. Inset pictures show the atomistic location of aluminum for the most active site in 8MR (upper) and the FESEM image of FER-S1 sample (lower). Reprinted with permission from [13] Copyright (2020) American Chemical Society.

alytic reactivity for DME carbonylation to MA [13] because recrystallization during the preparation step resulted in high crystallinity for many BAS in 8MR. In the subsequent study, the most active aluminum location that drastically enhanced the carbonylation rate was identified and the strength of the degree of the interaction between BAS and DME was calculated by first principles calculations, as shown in Fig. 1 [14].

Another important class of zeolites is ion-exchanged zeolites. Zeolites have the intrinsic ability to remove various ions from aqueous solutions, by either the adsorption of single-charged ions or the coadsorption of multiple-charged ions at Al- sites [15]; Exchange of hydrogen atoms with various metal cations such as Cu^{2+} and Ag^{+} can result in well-distributed single-atom catalytic sites. Wide application of ion-exchanged zeolites has been reported, including deNOx reactions for mobile vehicles [16].

Aluminum distribution is also important in ion-exchanged zeolites, as BAS distribution determines the number and location of active exchanged metal ions, and thus the catalytic activity. For example, it was reported that the location of BAS can significantly influence methane activation energy in Zn-exchanged MFI zeolite [17]. Li et al. also found rings with multiple BAS selectively accommodate Z_2Cu species, whereas rings with single BAS will tend to form ZCuOH as the dominant Cu exchange scheme in Cu exchanged zeolites (where Z stands for BAS) [18], again emphasizing the importance of BAS distribution on the active sites.

EFFECTS OF THERMODYNAMIC DISTRIBUTION OF Al AND BAS ON CATALYTIC PROPERTIES

Al is placed in zeolites according to the rules governed by thermodynamics and kinetics of the formation. One of the most famous rules is Löwenstein's rule, which states that the formation of Al-O-Al sequence is generally prohibited due to the energetics of formation [19-21].

Information on the thermodynamically stable sites of Al substitution and, more importantly, their distribution, provides valuable insight into the properties of zeolites. Since adsorption energetics, acidity, and stability can all be altered by the location of Al and BAS, it is crucial to know their probability of existence in the actual zeolites. Several studies that have performed extensive calculations of single and multiple substitutions on the unperturbed, thermodynamically preferable locations of Al are provided below.

Over the years, theoretical studies on zeolites have moved from simple cluster models to larger clusters or periodic structures [23-25]. Investigation of both single and multiple site substitutions and their influence is now being conducted based on different levels of theories, including molecular mechanics (MM), quantum mechanics (QM), and hybrid methods. Each method provides different levels of accuracy and scale of simulation.

Preferential Al locations and the consequent location of BAS can be determined by comparing relative energies to pure silicate frameworks. Some of the earlier studies used small and medium sized cluster models to calculate Al substitution energies [26]. By placing the BAS position of interest at the center and terminating by OH bonds, cluster models can be built as conducted in periodic zeolite frameworks. Although the small-sized cluster models provided relatively inexpensive means to determine the stable sites in the zeolite frameworks, they had limitations in accurately expressing the effects of paired Al sites. Therefore, either periodic models or medium-sized cluster models are better suited for discovering more detailed information on the distribution of Als in the zeolite frameworks at the expense of computational burden.

Investigation of all sites, including all combinations of paired sites, would produce the most accurate description of the preferential Al siting, although a substantial number of calculations are required, especially when two or more paired Al cases are considered. A way to address this problem of exponentially growing number of calculations would be to combine known scientific discoveries or apply the hypotheses such as Löwenstein's rule, to narrow down the sites of interest. He et al. investigated Al siting in periodic FER zeolites using a hybrid method based on the ONIOM code (our own N-layered integrated molecular orbital+molecular mechanics) [27]. Their calculations for the substitution and deprotonation energies of different configurations in all isolated T sites revealed that the T4 site was the most stable, with the T1 site as the second most stable (Fig. 2). In the case of two Al substitutions, the limited search space for a combination of T4 and T1 sites was considered. The Al4-O6-Si2 acid site was fixed because it was the most stable, while the other sites were varied for substitution. The most stable case was found to be the T4-O$(SiO)_2$-T4 site substitution, where the two T4 sites that were located in the same 6MR were replaced by Al, enabling intra-framework hydrogen bonds. They further suggested the hypothesis that in the case of FERs with high Al content, all T4 sites are filled before T1 sites.

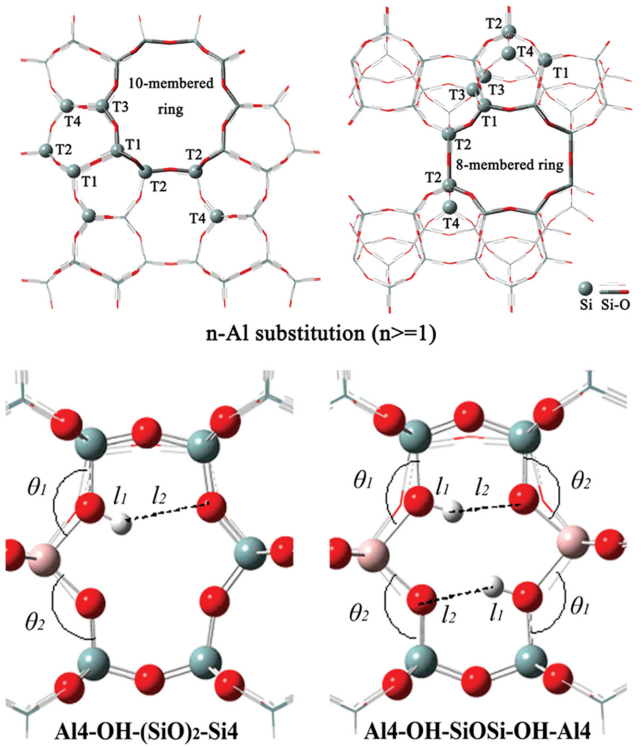

Fig. 2. The Al sites in FER zeolites (top) and two most stable configurations in single and double Al substitution as shown by He et al. [26].

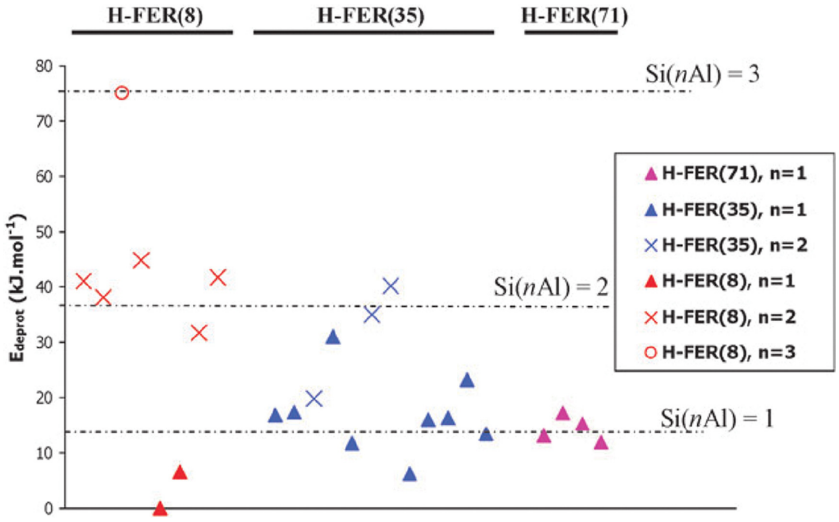

Fig. 3. Deprotonation energies against various configurations of Si/Al ratios and nth hydrogen deprotonation. Reprinted with permission from [28]. Copyright (2009) Royal Society of Chemistry.

Practical consideration can be given to finding the most stable sites and gain insight into the specific mechanisms effectively, narrowing down the search space of Al and BAS locations by applying certain hypotheses. However, the investigation of the nature of zeolites themselves requires more reliable proof regarding the location of Al distributions, and the resulting catalytic properties must be obtained by more exhaustive calculations. Grajciar et al. surveyed all possible isolated and paired sites of Al siting in H-FER zeolites with Si/Al ratios of 71 : 1, 35 : 1, and 8 : 1 [28]. The Si-O-Al vibrational frequencies of OH species (ν_{OH}) and deprotonation energies (DPEs) were obtained using periodic DFT calculations. They found that the Si-O-Al bond angle generally correlated with ν_{OH} with exceptions; intra-hydrogen bonded Brønsted acid sites derail from this correlation. A trend could be observed between the different ratios of Si/Al systems, where DPEs were high for highly Al substituted cases when averaged over subsequent configurations (Fig. 3). Although the results based on simple averaging may be trivial, they could still approximate the experimentally measured DPEs.

While Al substitution in frameworks may be governed partially by thermodynamic stability, the most preferred adsorption sites may differ from the most stable acidic sites, depending on adsorbate types as shown in [28]. Thus, various adsorption too must be asessed with statistical averaging. Such work has been demonstrated by Nystrom et al. where they applied statistical averaging to investigate dehydrogenation energy (DHE), DPE, and NH_3BE (ammonia binding energy) for all isolated and paired sites of Chabazite (CHA) zeolites [29]. They found that Al atoms up to 9 Å apart,

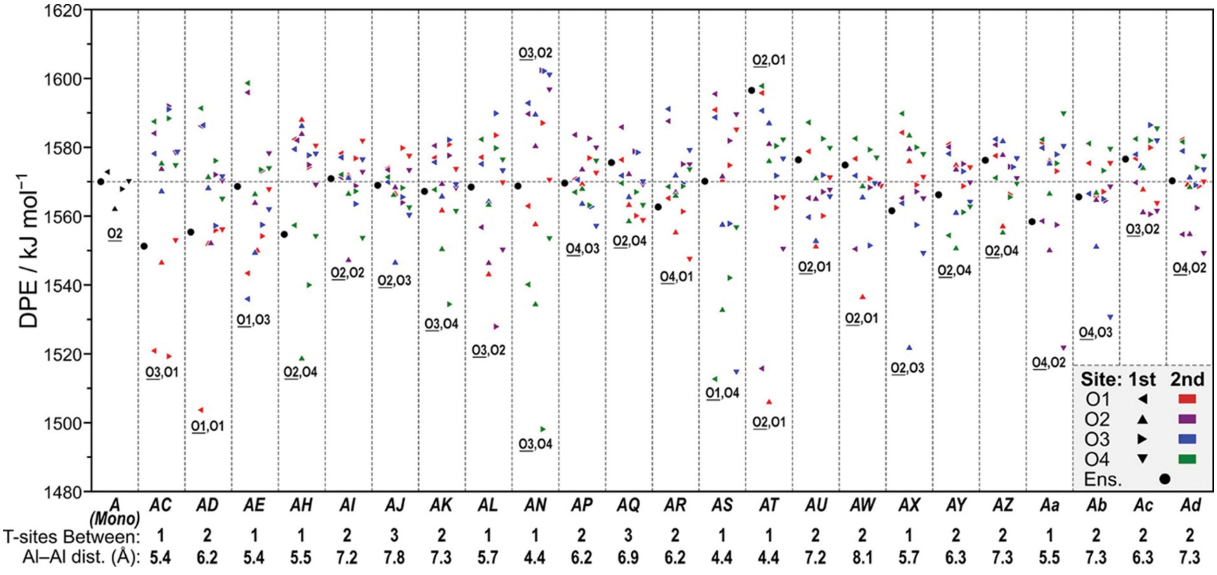

Fig. 4. Deprotonation energies for the isolated and all site-pairs when the second site is protonated. Ensemble averaged values are also shown; Reprinted (adapted) with permission from [29]. Copyright (2018) American Chemical Society.

that is, up to three linking Si-T sites, influence each other's acid site strengths. For example, two paired BAS in the 6-membered ring (6MR) will become stronger than those located in different rings due to the hydrogen bond interaction. Using periodic DFT calculations the Boltzmann and arithmetic averaged energies were obtained for the isolated and all 23 site pairs of Al siting. Since CHA zeolites have only one symmetrically distinct T site, it was possible to average in two axes across different O sites and different T sites. The average stability of the isolated hydrogen site was shown to be a good predictor of the location of the second hydrogen. Ensemble-averaged DPEs were very important for paired site motifs, as the difference from the lowest DPE was up to the order of ~10 kJ/mol. The sites that were calculated to be highly acidic were unlikely to exist because proton transfer would occur easily to satisfy the Boltzmann distribution of proton location. A second Al site stabilizes the conjugate base when placed in the proximity of the deprotonated site. For site pairs included in the same ring or in close proximity, a decline in DPE values was observed, attributed to the dipole-dipole interaction or hydrogen bond formation. As a result, a correlation between proton-anion distance and ensemble-averaged DPE was observed (Fig. 4). This trend was broken for the site pairs sharing the same 4-membered ring (4MR) due to significant strain effects. However, when NH_4^+ species substituted proximal proton sites, a reversal in trend was shown because NH_4^+ failed to stabilize the conjugate base in proximal Al siting and DPE values increased by up to 11 kJ/mol on average. Analysis of this phenomenon site by site showed that the degree of increase for the paired sites in the same 6MR was large (up to 40 kJ/mol higher DPE than that of the isolated sites), while the value was lowered by 10 kJ/mol for the site pairs within the same 8MR. This is attributed to the fact that NH_4^+ will stabilize the deprotonated sites if two BAS sites are located in the proximity of the same 8MR. Therefore, when BAS is occupied by different adsorbates, trends in acidity will change depending on the pore size, adsorbate size, and site proximity.

Although several studies have examined the thermodynamically stable distribution of BAS, the hypothesis that thermodynam-

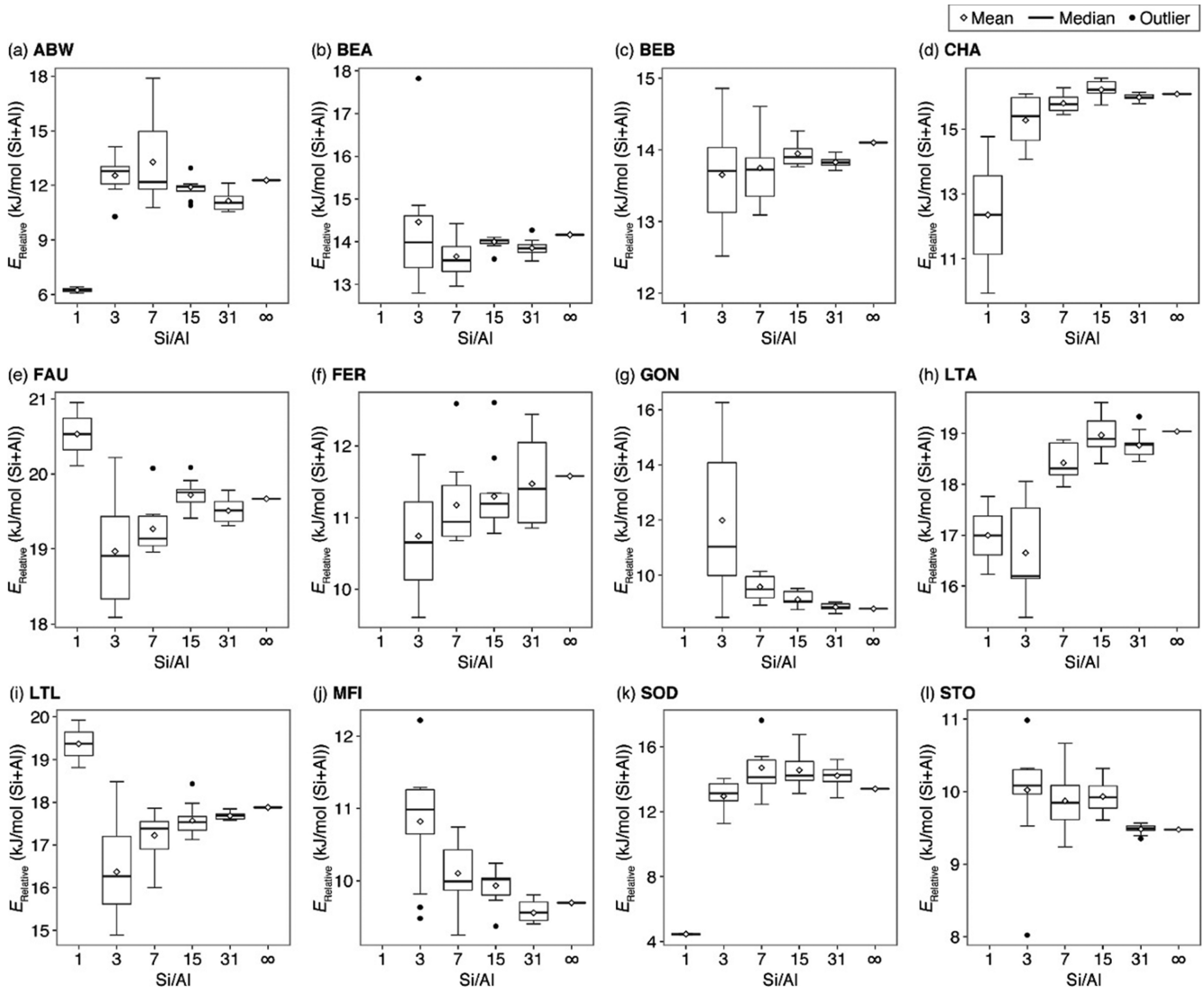

Fig. 5. Distribution of relative energies in different zeolite frameworks with varying Si/Al ratios. Reprinted with permission from [30]. Copyright (2016) American Chemical Society.

Table 1. Summary of computational approaches on evaluation of isolated & paired BAS

Methods	Representation	Zeolite framework(s)	# of structures	Calculated properties	References
QM/MM (ONIUM)	Cluster	H-FER	22	[a]E_{sub} DPE	[25]
DFT (PBE)	Periodic	H-FER	57	[b]∠SiOAl [c]ν_{OH} [d]ΔE_{rel}	[26]
DFT (RPBE)	Periodic	CHA	372	DPE DHE NH_3BE	[28]
MM (SLC potential)	Periodic	209 different frameworks	~43,000	[e]$E_{Framework}$, T-site density, ∠TOT	[29]

[a]Substitution energy, [b]Si-O(H)-Al angle, [c]O-H stretching frequency, [d]Relative binding energy, [e]Relative framework energy

ically stable Al siting correlates with actual siting in zeolites is difficult to prove, though it seems plausible by common sense. Such general statements can only be affirmed, or at least presumed to be true, after numerous cases have been examined and statistical significance has been demonstrated. Muraoka et al. applied a statistical approach to the data generated by molecular dynamics for 43,000 initial structures of different topologies, Al locations, and compositions [30]. They found that high Al content resulted in low density and large variance in energy, indicating that the change in Al location leads to a change in lattice energy. They compared the relative energies for different Si/Al ratios to find a linear scaling relationship. For low Si/Al ratio, the energetic variance regarding Al location increased. It was also found by investigating the relative stability of the Si/Al ratio for each type of zeolite framework that the differences in energy depend on the composition and topology (Fig. 5). For several selected zeolite topologies, a specific distribution of Als was found to be statistically more stable than random distributions, indicating that the Al siting and the synthesis of zeolites is governed by not only the kinetics but also the thermodynamics of Al substitution. Some computational works mentioned in this section have been summarized in Table 1.

SYNTHETICALLY CONTROLLED Al DISTRIBUTION

In the above sections, zeolites that follow the thermodynamically natural placement of Al were discussed. However, in most cases, different synthesis conditions are known to result in different distributions of Al, and many researchers have been seeking to exploit this feature, aiming to find ways to place Al on the preferential sites to enhance catalytic and mechanical properties. It has been reported that structure-directing agents (SDAs) can control the framework morphology; preferential aluminum placement is possible when charged SDAs are used.

The intrinsic activity of zeolites is determined by the distribution of BAS rather than the Si/Al ratio. Xu et al. synthesized Y zeolite with a Si/Al ratio of 3.6 by introducing sodium fluoride, while the synthesis without NaF resulted in a ratio of 3.3 [31]. Infrared spectroscopy (IR) and thermogravimetric analysis (TGA) were used

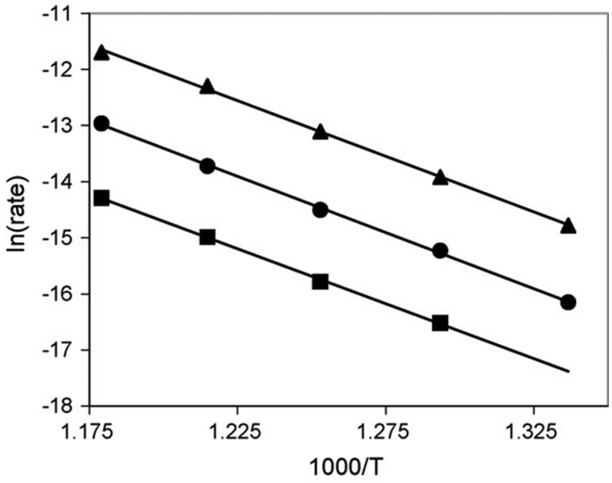

Fig. 6. Arrhenius plots of monomolecular cracking of propane over Y(2.6) (rectangle), Y(3.3) (circle), and Y(3.6) (triangle). Reprinted with permission from [31]. Copyright (2007) Elsevier.

to calculate the number of BAS samples. The catalytic activity of the monomolecular propane cracking was evaluated, and the Arrhenius plots were used to determine the reaction rate and activation energy (Fig. 6). As the Si/Al ratio increased, the cracking rates per weight of the catalyst also increased, while the activation energy remained constant. TGA and magic-angle spinning nuclear magnetic resonance (MAS-NMR) analysis revealed that the number of BAS increased in the order of Si/Al ratio of 2.6, 3.3, and 3.6, while the number of isolated BASs, which tended to be stronger acid sites than the paired ones, was in the reverse order. Therefore, it was concluded that the difference in cracking rates is attributed purely to the number of strong isolated BASs that take part in the reaction.

Another way to control the BAS location is the co-doping of other 3+ ions. The deliberate placement of a certain amount of BAS in the rings with the specified size and channels is key to the selectivity of the desired reactions. Cui et al. used a boron (B)-modification method in high-silica hierarchically structured ZSM-5 zeolite (HSZ) to control the distribution of framework Al [32].

Four zeolites with different B/Al ratio of 0, 3, 7, and 9 were synthesized using the steam-assisted crystallization (SAC) method, and the elemental content and acidity were measured by inductively coupled plasma optical emission spectrometry (ICP-OES) and NH_3 temperature-programmed desorption (NH_3-TPD), respectively. Cracking of 1-hexane was considered an excellent probe for locating the Al distribution. Al was more selectively located in the narrow straight/sinusoidal channels in samples with B/Al ratio of 7 and 9 than those of 0 and 3, and such placement of Al in the former samples promoted the methanol to olefin reaction cycle and elongated catalyst lifetime. This study demonstrates that synthesis methods such as boron modification can lead to a change in the framework Al distribution, which in turn affects the catalytic activity of the zeolite.

The distribution of Al atoms can also be controlled by the type of organic species used in the synthesis process. Park et al. synthesized ZSM-5 zeolites using two different organic species in a synthetic gel: tetrapropylammonium (TPA) cations and Na cations with pentaerythritol (PET, Na) [33]. The cracking of 1-octene was conducted over two ZSM-5 catalysts, and the activity was compared using the hydrogen transfer coefficient (HTC) and cracking mechanism ratio (CMR). The distribution of Al atoms and acid sites was estimated by MAS-NMR and constraint index (CI). They suggested that the Al of [PET, Na] was mainly located inside the 10-ring channels, while that in [TPA] was at the intersection between the channels, indicating that the distribution of Al atoms is well regulated by the organic species of the synthetic gel. [PET, Na] exhibited better catalytic activity and less coke formation, leading to durability than [TPA]. This work shows that a zeolite's catalytic performance and durability for coke formation is substantially influenced by the location of the acid sites.

Similar work has also been reported by Di Iorio et al., where the specific location of BAS could be synthetically controlled [34]. CHA zeolites with isolated Al sites could be synthesized using N,N,N-trimethyl-1-adamantylammonium cation (TMAda+) as an SDA. When cations with high charge density, such as Na^+, were used in conjunction with TMAda+ with a fixed total cation content, additional BAS could be incorporated in the same 6MR with the isolated site. Depending on the amount of Na^+ used, up to 44% of Al could be placed in the paired positions, defined as (Al-O(-Si-O)$_x$-Al) with ($x \leq 2$). Such characterization was conducted with divalent cobalt ion titration method. In the case of methanol dehydration to dimethyl ether, the first and zero-order methanol dehydration rate constants were ten times higher for the paired sites than for the isolated sites.

It is difficult to exactly locate Al atoms, especially when complex synthesis methods are involved. Sastre et al. used force-field atomistic simulation to determine the Al distribution in ITO-7, in conjunction with experiments [35], where ITO-7 was synthesized with $C_{14}H_{26}NOH$ as the OSDA. Under the hypothesis that SDAs are sterically fixed at the configuration in neutral silicate pores, they computed relative energies for different Al sitings and BAS positions and found that the ensemble-averaged ν_{OH} with SDAs included was close to that of IR experiments. When the SDA was excluded, only one hydroxyl band appeared, as opposed to the case where the SDAs were included (Fig. 7).

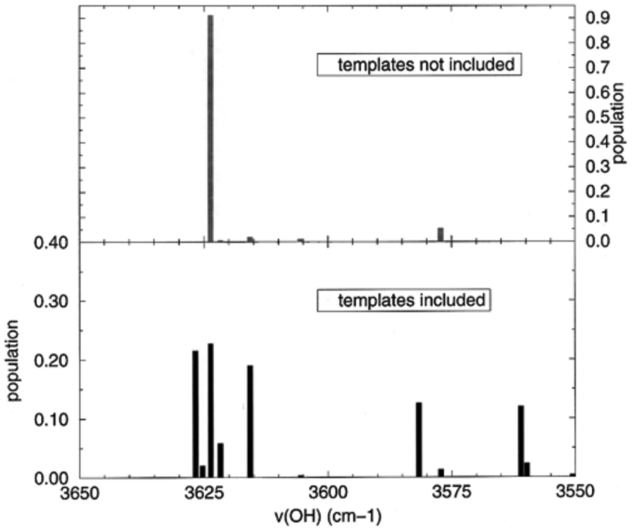

Fig. 7. The calculated force field concerning the Boltzmann averaged OH frequencies in H-ITQ-7 without (top) and with (bottom) SDA. Reprinted with permission from [35]. Copyright (2002) American Chemical Society.

DEALUMINATION

Dealumination occurs when severe conditions such as high temperature and low pH are applied to the aluminosilicates, whether post-processing reaction or catalytic regeneration process. Al atoms at T sites are dealuminated via acidic or hydrothermal reactions, where acids or water molecules interact with the aluminosilicate framework to break the T-O bond, respectively.

Although dealumination caused the loss of BAS and consequently the catalytic activity [36], it is often carried out intentionally as a post-synthetic treatment of zeolites to enhance the framework stability and resistivity to coke formation. Although statistical averaging methods have yet been implemented in dealuminated and consequently defect-induced zeolites, dealumination has taken place as a major post-processing method that possibly alters Al siting and composition, and thus, some recent works on this topic are introduced for the sake of completeness.

Inagaki et al. applied vapor-phase $TiCl_4$ treatment on ZSM-5 at 600 °C [37] and combined QM/MM calculations with Al MAS-NMR measurements to probe the distribution of the Al sites. After the post-synthtic treatment, Al NMR peak moved from 55 to 52 ppm, indicating that the selective dealumination of the framework Al species occurred at 55 ppm. The measured FT-IR spectra with pyridine adsorption on the samples indicated Ti/ZSM-5(600) had weaker acidic strength than the parent ZSM-5, attributed to the $TiCl_4$ treatment reducing the number of strong BAS. Consequently, Ti/ZSM-5(600) showed lower conversion for both ethylene-to-propylene reaction and cumene cracking than the parent ZSM-5, while the stability of the samples increased, as can be seen in Fig. 8.

Korányi et al. presented a theoretical model using the periodic building unit (PBU) [38]. Although no simulations were conducted, they evaluated the effect of Al siting after dealumination using MAS-NMR spectroscopy and cross-polarization (CP) measure-

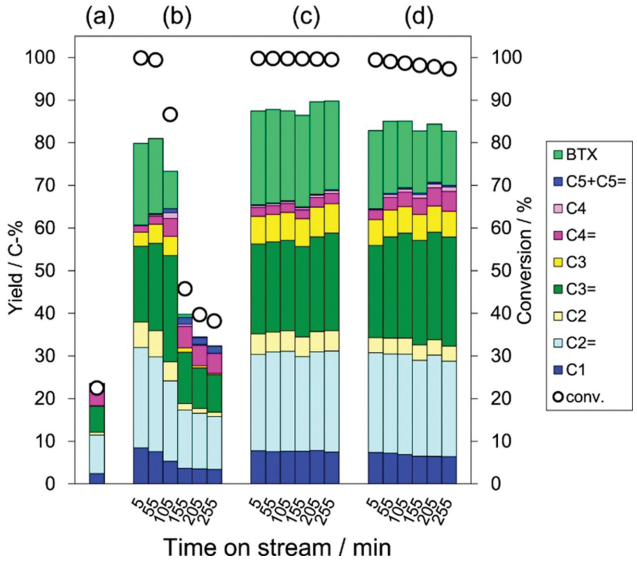

Fig. 8. Hexane conversion and product yield (C-%) for hexane cracking over original and steam processed zeolites. The reactions were carried out (a) without catalysts and with (b) parent ZSM-5, (c) AT-ZSM-5, and (d) Ti/ZSM-5(600). Reprinted from [37]. Copyright (2020) Elsevier.

ments. The NMR signal intensities of zeolites with various Si/Al ratios were decomposed to the contributions from Si(nAl) and Si(OH)x sites to predict the concentration of Al siting and defected sites, respectively. By building the PBUs of MOR (12 atoms) and beta (BEA, 16 atoms) zeolites under the assumptions that only certain configurations of PBU, namely twin (two Al per PBU), lone (one Al per PBU), and silicate are energetically favorable, they calculated the concentration of each distinct site in the PBUs and compared the results with the NMR intensity peaks to show that the dealumination process occurred in both twin and single Al PBUs. This work corroborated the effectiveness of the method that theoretically built a picture of Al siting and suggested that the previously reported hypothesis for the involvement of only two by two Al siting in dealumination should be revised.

Although the exact Al siting after dealumination is still elusive, recent studies have uncovered the mechanism behind the dealumination process. Stanciakova et al. addressed the hydrothermal dealumination process in a model system of ZSM-5 using periodic DFT calculations [39] and reported four possible reaction mechanisms whose kinetics were dependent on temperature and partial pressure of water. When three different motifs of Al positions were compared, the accessibility of the substituted site was found to be a more important factor for the stability than the Al-O bond strength, with aluminum atoms in straight channels being the most stable.

QUANTIFICATION OF Al DISTRIBUTION THROUGH EXPERIMENT AND SIMULATIONS

Though the thermodynamic distribution of Al within frameworks can be calculated by simulations, the computed evidence must be linked to experimental observations to validate its effectiveness. The quantity and existence of different site distribution can be measured via spectroscopic methods. Many different applications have been developed in utilizing Si and Al magic angle spectroscopic (MAS NMR) chemical shifts. The most direct approach to gain insight into specific Al T-site distribution is using DFT to calculate analogous theoretical chemical shifts for each T site or pairs of T sites. Allocating the experimental peaks to that of DFT calculated peaks, the specific local environment of each Als can be determined. The chemical shifts then can be used to obtain distribution of sites in experimental catalysis.

Measurement and calculation of vibrational frequencies can be used to distinguish different Al distribution patterns. For example, Sklenak et al. distinguished three possible paired Al sitings of cationic sites [40]. Using Co and Cu exchanged FERs, NO stretching frequencies were determined via experimental FTIR spectroscopy and theoretically with DFT and MD calculations. NO molecules are common probes for analyzing local environments of their adsorbents which are the exchanged Co and Cu species in this case. Three AlO-$(SiO)_2$-Al sequences in different 6MR environments were investigated for cationic exchange where other possible sites and Al sequences were neglected with low energetic preference and experimental evidence of non-existence in ^{29}Si MAS NMR results [41]. Interestingly, when NO frequencies were obtained from DFT relaxed structures for Cu exchanged FERs, the stretching frequencies could not be properly assigned to their experimental counterpart, which is attributable to the fact that the exchange of metal ions induces structural rearrangement of 6 MRs depending on the Al placement, and the discrepancies disappeared only after molecular dynamics simulations were applied. This example shows that after proper treatment, theoretical calculations can be used in conjuncture with experimental FTIR data for detecting Al distribution. Similar works that utilized ^{27}Al MAS for the quantification of Al siting preferences in T sites, depending on the crystallization process, have also been reported [42]. A more detailed review of the methods integrating experimental observation with computational methods can be referred to as the reference [43].

EVALUATION OF EXPERIMENTAL DATA

Computer-simulated atomistic calculations can be more firmly linked to experimental data by statistical averaging. Some reported works focused on the evaluation of experimental data and deepened our understanding of what experimental analysis can provide by altering the common perceptions of several experimental properties.

Jones and Iglesia challenged some of the experimentally measured properties that were commonly perceived as indicators of acidity [44]. They calculated the most stable hydrogen location, ensemble-averaged DPE values, ν_{OH}, Si-O-Al bond angle, and ammonia heat of adsorption for all the structures of different Al siting in six different zeolite frameworks. The vast amount of calculations in their work showed that the variation in DPE values was insignificant between the six different zeolite frameworks. The ensemble-averaged DPE values were largely uncorrelated to the rest of the properties obtained, and the DPE values were correlated to the geometric/steric effects that promote the reaction via the relaxation of the transition phase. More specifically, the ν_{OH}, Si-O-Al

angle, and ammonia heat of adsorption were found to be uncorrelated to ensemble-averaged DPE values, which is in conflict with the historically common belief [45]. Meanwhile, ν_{OH} showed a correlation with the confinement factors, meaning that the stability of the conjugate anion is a dominant factor for ν_{OH}. They also analyzed all approachable sites in H-MFI samples and found that many of the adsorption moieties of NH_3 were predominantly relaxed by dispersion energy, in contrast to the common sense that the heat of ammonia adsorption is substantially influenced by the acidic strength of BAS. The accuracy of theoretical ammonia adsorption enthalpies was corroborated by comparison with microcalorimetry experiments.

They also refuted the claim that the correlation of NH_3 adsorption energies with turnover frequencies, as reported in some experimental works because the stability of transition states (TS) was found to be significantly influenced by steric effects. Using the formulation of an averaged activation enthalpy by the transition state theory, in analog to the ensemble-averaged proton siting in their zeolite frameworks, they found that the DPE values were independent of the Al site location and zeolite frameworks, and thus inferred that the difference in activation enthalpies for each case resulted from the dispersive and H-bonding interactions of the TS configuration.

As discussed above, the heat of ammonia adsorption is largely influenced by factors such as van der Waals interactions, preventing it from being used as an accurate measure of BAS acidity. However, such adsorption measurements may still provide information about the catalytic activity. For example, Wang et al. found that there existed scaling relations between ammonia adsorption enthalpy and propene methylation activation energy in metal-substituted CHA and ALPO-34 zeolites [46]. Such scaling relations were especially useful as the ΔH determined by computation could be directly used for consecutive microkinetic analysis to predict turnover frequencies. For some specific cases, the adsorption of such probe molecules could serve as a descriptor for reactivity. Boronat et al. [47] conducted a comprehensive study to use the measured adsorption energy of probe molecules by calorimetry as an indicator of the acidity and catalytic activity. However because many theoretical studies have reported that deprotonation energies vary by less than 30 kJ/mol for each zeolite, other factors such as the confinement effect on the protonated species play an important role [6]. They applied periodic DFT and measured the interaction energies of adsorbed probe molecules (CO, CH_4, NH_3, pyridine) with pure and single Al-incorporated MOR and ZSM-5 zeolites. This allowed the separate evaluation of the pore size effect and proton transfer process. Because weak base molecules might be weakly adsorbed and fail to deprotonate hydrogen, the ZH-B neutral complex was measured rather than an electron transferred Z^--HB^+ state. For strong bases, the measured heat of adsorption was not necessarily dependent on the acidity but on the steric effects; thus, the extent to which the Z^--BH^+ ion pair was stabilized by the oxygen atoms in the vicinity. Since steric effects are involved in the adsorption of both weak and strong bases, it can be concluded that probe molecules should be used for the information about confining voids rather than evaluating the acidity of the catalysts.

MACHINE LEARNING TO ESTIMATE THE CATALYTIC PROPERTIES OF ZEOLITES

Although the combination of atomistic simulation and statistical treatment has narrowed the quantitative gap between simulated and experimental evaluations, computational limits still restrict either the search space or the level of accuracy of the evaluations. Machine learning (ML) has emerged as a solution to address such problems in the broad spectrum of heterogeneous catalysts. While DFT calculations only give pointwise information in parameter space, integration of machine learning enables fast prediction on the whole landscape, while retaining the accuracy of quantum mechanical calculations. Statistical averaging of the vast information from ML predictions will potentially produce a highly accurate description of actual zeolite properties, with a substantially reduced computational workload.

Despite the promising application of ML techniques to many fields of catalysts, few studies have yet been conducted to integrate them in the area of zeolite sciences, with the focus mostly on predicting non-catalytic properties using non-local descriptors. In this section, some recent studies utilizing ML to analyze and discover zeolites are summarized, along with examples of studies conducted on other heterogeneous catalysts to depict future perspectives in ML for zeolites.

1. Machine Learning Applied to Framework-wise Properties

Evans and Coudert used simple machine learning techniques to predict the mechanical properties of zeolite frameworks [48]. The DFT optimized frameworks of 121 pure silica zeolites were used as training data to predicted logarithms of bulk and shear moduli (log(K) and log(G), respectively) of zeolite frameworks using 32 different descriptors encompassing the local, structural, and porosity of each framework. The cross-validation accuracy was shown to be within RMSE of 0.102±0.034 and 0.0847±0.022 for log(K) and log(G), which is an improvement compared to conventional force field models. They then extended their model to predict 500,000 different hypothetical and real frameworks, and extract the notion that real zeolites tend to be stiffer than the hypothetical ones, discovering a new criterion for assessing synthesis feasibility.

Gu et al. constructed a model for nitrogen adsorption on various zeolite frameworks using the feature learning approach to extract knowledge of the improved representations of zeolites [49]. Since adsorption on porous zeolites strongly depends on structural accessibility as well as energetic property, the authors considered 13 input features concerning local, structural, channel-related information. Applying Pearson correlation analysis, they built smaller models by first removing five redandant features (eight feature model), and further removing five highly correlated features (three feature model). When the reduced model was applied to the dataset of 248 zeolites, the XGBoost algorithm performed best where the R-square value of binding energy predictions were 0.77, 0.94, and 0.92 for the cases with 13, 8, and 3 features, respectively. The remaining three principal features were the maximum number of nitrogens that could be accommodated in a pore (V_{eff}), the largest sphere that can be included in the existing channels (PLD), and the refinement distance least squares (R_{DLS}) which encodes the average distance of Si-Si, Si-O, and O-O bonds. While the initial

dataset consisted of pure silicate frameworks, the authors applied their three feature model to Al-containing zeolites by introducing a scaling coefficient and demonstrated that the model can successfully generate adsorption isotherms similar to those obtained from experiments.

While the strength of feature learning is that it extracts human interpretable information, one of the important advantages of applying machine learning to chemical domains is its ability to construct nonlinear surrogate models, by which more powerful hidden features (which may be non-human readable) can be discovered in the process. Helfrecht et al. used smooth overlap of atomic positions (SOAP) as local descriptors, using kernel ridge regression (KRR) model to predict molar volume and cohesive energy of hypothetical zeolite frameworks in the Deem database [50]. The method showed marginally improved performance compared to that by classical descriptors such as Si-Si distance and Si-O-Si angle. They then reduced the dimensionality of SOAP descriptors through kernel principal component analysis (kPCA) and used the three principal components to construct a 3D cloud atlas of all hypothetical zeolite frameworks, with the power of representing diverse structural motifs in the database.

2. Local Descriptors for Zeolite Representation

While the previously mentioned models used information of each zeolite framework to predict general framework-wise properties, many machine learning and deep learning approaches built the models that encoded local site information to predict the property specific to local activity. In this respect, the representation of atomic and bond-wise information for crystals, molecules, and adsorbates has been a key factor for researchers. Over the years, simple descriptors such as generalized coordination numbers (GCN) and orbital-wise coordination numbers have been proposed to successfully predict adsorption energy in simple metallic catalysts, even without machine learning techniques [51,52].

However, such descriptors are limited to description of surfaces of metal catalysts, and demand for more general models applicable to wider domains has existed. Machine learning-based models can utilize the descriptors based on more detailed information, especially the local information, and many approaches have been developed for heterogeneous surfaces. Meanwhile, to our knowledge, only SOAP descriptors have been applied to zeolites because the representation of zeolites is potentially more complex than other heterogeneous catalysts; in other words, the active sites are within three-dimensionally surrounded frameworks. For example, it is hard to predict the energetics of adsorption on each site because adsorption energies are closely linked to not only the very adjacent atoms but also the ring and pore atoms which may interact with the adsorbate by van der Waals force. Likewise, the complexity in the structure of zeolites makes the prediction of activation energy substantially complicated, as the accommodation of transition states in pores becomes even more important. Therefore, a novel representation that can consider not only the local but also the 3D structural environment around the active site must be developed.

Graph representation methods, where nodes and edges are used to encompass atomic information (atomic numbers, electronegativity, etc.) and the relations between atoms (bond length, type), respectively, have been shown to be appropriate to estimate bulk [53], surface and adsorption properties [54,55]. Graph representations utilize graph convolutional networks, also known as the message passing networks, where information of each node is passed as 'messages' to the connected nodes in each convolution, making each node collate information of its n^{th} neighbors. Graph methods may apply to the prediction of interactions between the zeolite framework and small molecules in large rings where interpore interactions are negligible. For more general application at the existence of interpore interactions, modification of current models might be needed by taking the hydrogen bonds and van der Waals interaction into account. While current models use various methods such as distances and Voronoi solid angles to encode bonding information, expansion of edge properties to subtle interactions may be needed or implemented by a separate model.

To encode 3-dimensional information, kernel methods such as SOAP can be used to analyze local environments, by using kernel distances as a measure of similarity between the atomic neighbor environments. SOAP uses the expansion of atomic density to express local geometries in a smooth and transformation invariant form, using Gaussian neighbor density. One of the advantages of SOAP is that different atomic environments can be compared by constructing normalized matrix multiplications for kernel distance between each environment, and learning only the weights on each kernel. SOAP has been applied to the development of machine learning potential for a variety of applications, including the prediction of silicon surface reconstruction, molecular atomization energy on the QM7b database, and framework-wise property of zeolites, as introduced in the preceding section [50,56].

Recently, Kajita et al. proposed to use 3D voxels for representing atomic positions of solid state meterials [57]. For periodic materials, a cell can be transferred to reciprocal space using Fourier transformation, as used in DFT methods. The use of reciprocal space solves many problems in representing periodic materials, such as translational invariance, unit cell selection, and atomic label commutation. The one remaining problem of rotational invariance can be solved by data augmentation, simply including various rotated structures of the same material in the dataset. Because the descriptor is inherently similar to pixel data, algorithms such as convolutional neural networks (CNN), originally developed for machine vision purposes, can be directly applied. 3D voxels have been applied to generation and screening of stable oxide structures when used along with generative models.

As zeolites are highly periodic, the use of voxels can potentially be beneficial in determining zeolite catalytic properties. When additional fast optimization methods such as MM, or recently developed machine learning optimizers are used along with 3D voxels, more accurate initial positions can be generated [58], increasing the practicality of the method.

CONCLUSIONS

This review depicts the recent developments in the field of zeolite sciences, with emphasis on computational methods to explain and supplement experimental analyses. The importance of Al and BAS distribution has been discussed via the reviews on the reported

works by showing that computational methods, more specifically statistical averaging, have estimated thermodynamically preferential Al siting and discovered the consequent effects of BAS distribution. Computational studies to evaluate the effects of paired Al sites have been conducted for different zeolite frameworks extensively, and have successfully described the generalized properties, indicating that theories are expected to play a useful role in designing a zeolite with the desired Al distribution, in collaboration with experimental works. However, many studies are limited to the information on the selected zeolites of interest, and the knowledge of different zeolite frameworks and their catalytic performance has been accumulated in a fragmented fashion.

Despite the great improvement in computational studies, further developments are still needed to incorporate the synthesis and deactivation of zeolites, as the crystallization process and defect creation are yet to be fully understood or modeled. Data-driven methods are creating new paradigms, and the analysis of different zeolite structures is now possible. While the current focus has been limited to very simple properties such as DPE and vibrational frequencies, more complex properties such as adsorption and reaction of C1 and C2 molecules need to be predicted to effectively discover novel catalysts, via the simplification of search space in terms of either the catalyst framework or adsorbate molecules. This can be accomplished by finding general structure-activity relationships in catalyst frameworks or adequate reactivity descriptors in adsorbate molecules.

Overall, future trends are directed toward a more extensive computational search along with its integration with experimental studies, to understand the governing mechanism of zeolites and design better ones. Execution of computational search seems promising by integrating ML techniques to accelerate and widen the possible search domains.

ACKNOWLEDGEMENTS

This work was supported by the C1 Gas Refinery Program through the National Research Foundation of Korea (NRF), funded by the Ministry of Science, ICT & Future Planning (No. NRF-2018M3D3A1A01055765).

REFERENCES

1. D. W. Breck, in *Molecular sieve zeolites-I*, E. M. Flanigen and L. B. Sand Eds., ACS Publications, Washington D.C. (1971).
2. C. Baerlocher and L. B. McCusker, Database of zeolites, http://www.iza-structure.org/databases/ (accessed November 4, 2020).
3. Q. Zhang, J. Yu and A. Corma, *Adv. Mater.*, **2002927**, 1 (2020).
4. Y. Chu, B. Han, A. Zheng and F. Deng, *J. Phys. Chem. C.*, **116**, 12687 (2012).
5. Y. Huang, X. Dong, M. Li and Y. Yu, *Catal. Sci. Technol.*, **5**, 1093 (2015).
6. M. Brändle and J. Sauer, *J. Am. Chem. Soc.*, **120**, 1556 (1998).
7. D. A. McQuarrie, Statistical Mechanics, 1st Ed., Harper & Row, New York (1973).
8. P. Cheung, A. Bhan, G. J. Sunley and E. Iglesia, *Angew. Chem. - Int. Ed.*, **45**, 1617 (2006).
9. P. Cheung, A. Bhan, G. J. Sunley, D. J. Law and E. Iglesia, *J. Catal.*, **245**, 110 (2007).
10. A. Bhan, A. D. Allian, G. J. Sunley, D. J. Law and E. Iglesia, *J. Am. Chem. Soc.*, **129**, 4919 (2007).
11. M. Boronat, C. Martínez-Sánchez, D. Law and A. Corma, *J. Am. Chem. Soc.*, **130**, 16316 (2008).
12. Y. Li, M. Yu, K. Cai, M. Wang, J. Lv, R. F. Howe, S. Huang and X. Ma, *Phys. Chem. Chem. Phys.*, **22**, 11374 (2020).
13. H. S. Jung, H. Ham and J. W. Bae, *Catal. Today*, **339**, 79 (2020).
14. H. Ham, H. S. Jung, H. S. Kim, J. Kim, S. J. Cho, W. B. Lee, M. J. Park and J. W. Bae, *ACS Catal.*, **10**, 5135 (2020).
15. J. Perić, M. Trgo and N. Vukojević Medvidović, *Water Res.*, **38**, 1893 (2004).
16. H. Yahiro and M. Iwamoto, *Appl. Catal. A Gen.*, **222**, 163 (2001).
17. S. C. Albarracín-Suazo, Y. J. Pagán-Torres and M. C. Curet-Arana, *J. Phys. Chem. C.*, **123**, 16164 (2019).
18. H. Li, C. Paolucci, I. Khurana, L. N. Wilcox, F. Göltl, J. D. Albarracin-Caballero, A. J. Shih, F. H. Ribeiro, R. Gounder and W. F. Schneider, *Chem. Sci.*, **10**, 2373 (2019).
19. W. Loewenstein, *Am. Mineral.*, **39**, 92 (1954).
20. C. R. A. Catlow, A. R. George and C. M. Freeman, *Chem. Commun.*, **11**, 1311 (1996).
21. A. G. Pelmenschikov, E. A. Paukshtis, M. O. Edisherashvili and G. M. Zhidomirov, *J. Phys. Chem.*, **96**, 7051 (1992).
22. T. J. Goncalves, P. N. Plessow and F. Studt, *ChemCatChem.*, **11**, 4368 (2019).
23. S. A. Zygmunt, L. A. Curtiss, P. Zapol and L. E. Iton, *J. Phys. Chem. B.*, **104**, 1944 (2000).
24. A. Kessi and B. Delley, *Int. J. Quantum Chem.*, **68**, 135 (1998).
25. D. Zhou, Y. Bao, M. Yang, N. He and G. Yang, *J. Mol. Catal. A Chem.*, **244**, 11 (2006).
26. M. He, J. Zhang, R. Liu, X. Sun and B. Chen, *Catalysts*, **7**, 11 (2017).
27. L. Grajciar, C. O. Areán, A. Pulido and P. Nachtigall, *Phys. Chem. Chem. Phys.*, **12**, 1497 (2010).
28. N. Zhang, C. Liu, J. Ma, R. Li and H. Jiao, *Phys. Chem. Chem. Phys.*, **21**, 18758 (2019).
29. S. Nystrom, A. Hoffman and D. Hibbitts, *ACS Catal.*, **8**, 7842 (2018).
30. K. Muraoka, W. Chaikittisilp and T. Okubo, *J. Am. Chem. Soc.*, **138**, 6184 (2016).
31. B. Xu, S. Bordiga, R. Prins and J. A. van Bokhoven, *Appl. Catal. A Gen.*, **333**, 245 (2007).
32. N. Cui, H. Guo, J. Zhou, L. Li, L. Guo, Z. Hua, *Micropor. Mesopor. Mater.*, **306**, 110411 (2020).
33. S. Park, T. Biligetu, Y. Wang, T. Nishitoba, J. N. Kondo and T. Yokoi, *Catal. Today*, **303**, 64 (2018).
34. J. R. Di Iorio, C. T. Nimlos and R. Gounder, *ACS Catal.*, **7**, 6663 (2017).
35. G. Sastre, V. Fornes and A. Corma, *J. Phys. Chem. B.*, **106**, 701 (2002).
36. M. Nielsen, A. Hafreager, R. Y. Brogaard, K. De Wispelaere, H. Falsig, P. Beato, V. Van Speybroeck and S. Svelle, *Catal. Sci. Technol.*, **9**, 3721 (2019).
37. S. Inagaki, N. Yamada, M. Nishii, Y. Nishi and Y. Kubota, *Micropor. Mesopor. Mater.*, **302**, 110223 (2020).
38. T. I. Korányi and J. B. Nagy, *J. Phys. Chem. B.*, **109**, 15791 (2005).

39. K. Stanciakova, B. Ensing, F. Göltl, R. E. Bulo, B. M. Weckhuysen, F. Gö, R. E. Bulo and B. M. Weckhuysen, *ACS Catal.*, **9**, 5119 (2019).
40. S. Sklenak, P. C. Andrikopoulos, S. R. Whittleton, H. Jirglova, P. Sazama, L. Benco, T. Bucko, J. Hafner and Z. Sobalik, *J. Phys. Chem. C.*, **117**, 3958 (2013).
41. S. Sklenak, P. C. Andrikopoulos, B. Boekfa, B. Jansang, J. Nováková, L. Benco, T. Bucko, J. Hafner, J. Ddeek and Z. Sobalík, *J. Catal.*, **272**, 262 (2010).
42. S. Kim, G. Park, M. H. Woo, G. Kwak and S. K. Kim, *ACS Catal.*, **9**, 2880 (2019).
43. B. C. Knott, C. T. Nimlos, D. J. Robichaud, M. R. Nimlos, S. Kim and R. Gounder, *ACS Catal.*, **8**, 770 (2018).
44. A. J. Jones and E. Iglesia, *ACS Catal.*, **5**, 5741 (2015).
45. P. J. O'Malley and J. Dwyer, *J. Phys. Chem.*, **92**, 3005 (1988).
46. C. M. Wang, R. Y. Brogaard, B. M. Weckhuysen, J. K. Nørskov and F. Studt, *J. Phys. Chem. Lett.*, **5**, 1516 (2014).
47. M. Boronat and A. Corma, *ACS Catal.*, **9**, 1539 (2019).
48. J. D. Evans and F. X. Coudert, *Chem. Mater.*, **29**, 7833 (2017).
49. Y. Gu, Z. Liu, C. Yu, X. Gu, L. Xu, Y. Gao and J. Ma, *J. Phys. Chem. C.*, **124**, 9314 (2020).
50. B. A. Helfrecht, R. Semino, G. Pireddu, S. M. Auerbach and M. Ceriotti, *J. Chem. Phys.*, **151**, 154112 (2019).
51. X. Ma and H. Xin, *Phys. Rev. Lett.*, **118**, 1 (2017).
52. F. Calle-Vallejo, J. I. Martínez, J. M. García-Lastra, P. Sautet and D. Loffreda, *Angew. Chem. - Int. Ed.*, **53**, 8316 (2014).
53. T. Xie and J. C. Grossman, *Phys. Rev. Lett.*, **120**, 145301 (2018).
54. G. H. Gu, J. Noh, S. Kim, S. Back, Z. Ulissi and Y. Jung, *J. Phys. Chem. Lett.*, **11**, 44 (2020).
55. S. Back, J. Yoon, N. Tian, W. Zhong, K. Tran and Z. W. Ulissi, *J. Phys. Chem. Lett.*, **10**, 4401 (2019).
56. S. De, A. P. Bartók, G. Csányi and M. Ceriotti, *Phys. Chem. Chem. Phys.*, **18**, 13754 (2016).
57. S. Kajita, N. Ohba, R. Jinnouchi and R. Asahi, *Sci. Rep.*, **7**, 1 (2017).
58. J. Yoon and Z. W. Ulissi, *Phys. Rev. Lett.*, **125**, 173001 (2020).